

# The magic of entangled top quarks

CHRIS D. WHITE<sup>a1</sup> AND MARTIN J. WHITE<sup>b2</sup>

<sup>a</sup> Centre for Theoretical Physics, School of Physical and Chemical Sciences,  
Queen Mary University of London, 327 Mile End Road, London E1 4NS, UK

<sup>b</sup> ARC Centre of Excellence for Dark Matter Particle Physics & CSSM,  
Department of Physics, University of Adelaide, Adelaide, SA 5005, Australia

## Abstract

Recent years have seen an increasing body of work examining how quantum entanglement can be measured at high energy particle physics experiments, thereby complementing traditional table-top experiments. This raises the question of whether more concepts from quantum computation can be examined at colliders, and we here consider the property of *magic*, which distinguishes those quantum states which have a genuine computational advantage over classical states. We examine top anti-top pair production at the LHC, showing that nature chooses to produce magic tops, where the amount of magic varies with the kinematics of the final state. We compare results for individual partonic channels and at proton-level, showing that averaging over final states typically increases magic. This is in contrast to entanglement measures, such as the concurrence, which typically decrease. Our results create new links between the quantum information and particle physics literatures, providing practical insights for further study.

## 1 Introduction

It has long been known that there are fundamental limits to the power of classical computers, so that they are unable to efficiently simulate the quantum world we live in [1]. This in turn led to the development of universal quantum computers, replacing the universal Turing machines of classical computation (see e.g. ref. [2] for a pedagogical review). It is an active field of research to experimentally realise large-scale quantum computers, and the parallel field of quantum information theory aims to quantify how information can be encoded, transmitted and corrected for errors. If quantum computers are to become a reality, it is imperative that algorithms for quantum computation be fault tolerant, and thus able to cope with potentially noisy communication channels.

As well as practical applications, quantum computing and / or information is also studied in the context of fundamental tests of quantum mechanics itself, and there is therefore widespread interest in finding novel physical systems which manifest quantum concepts and behaviour. To this

---

<sup>1</sup>christopher.white@qmul.ac.uk

<sup>2</sup>martin.white@adelaide.edu.au

end, an increasing body of work in recent years has examined quantum entanglement signatures at particle collider experiments such as the *Large Hadron Collider (LHC)*. Gains for particle physics include new signatures for disentangling new physics from the Standard Model. For quantum theorists, collider physics offers an unprecedentedly high energy regime in which to test their ideas. In this paper, we will focus on a particular scattering process at the LHC, namely the production of top-antitop quark pairs. The top quark is the heaviest known fundamental particle, and thus a potentially clear window through which to view new physics. It is also unique among the quarks in that it decays before it has a chance to hadronise, so that its kinematic properties (such as its spin) can be efficiently measured. Given that the top quark has spin  $1/2$ , a produced system of a top quark and an antitop quark constitutes a *two-qubit system* in the parlance of quantum information theory. Its use as a probe of quantum entanglement at the LHC was first proposed in ref. [3, 4], resulting in much follow-up work: see e.g. refs. [4, 5, 5–17] for theoretical studies relating to the top sector alone, and refs. [18–20] for experimental work from both the ATLAS and CMS collaborations. A thorough and pedagogical recent review of both theory and experiment is that of ref. [21].

Work to date has typically focused on the entanglement of (anti-)top spins, and whether this can be convincingly measured. One may also consider new physics corrections (e.g. expressed in the model-independent language of effective field theory [5]), to see whether measured entanglement can provide clear signatures of theories beyond the Standard Model. However, and as we will review in detail below, entanglement is not the only property characterising quantum systems, a point which has also been made in a top-related context in ref. [10]. A fruitful interplay between the fields of quantum computing and high energy physics should involve finding other interesting quantum information theoretic quantities, and seeing why and how these manifest themselves in a collider setting.

In this paper, we will examine a property called *magic* which, roughly speaking, measures whether quantum states possess a computational advantage over classical states. The study of magic is pivotal to such questions as how to make fault-tolerant quantum computers (see e.g. [2]), and various studies have addressed how to properly quantify this concept [22–32]. Given the recent nature of much of this work, it seems particularly timely to explore whether the property of magic is a natural inevitability at current collider experiments. Put more simply: does nature produce magic top quarks and, if not, why not? Such questions are conceptually interesting in their own right perhaps, but may also clarify how to exploit magic in other naturally occurring quantum systems. Going the other way, collider analyses provide an experimental playground for developing insights into quantum information theory. Crucial for this is that we can map concepts from quantum computation to collider physics, and appreciate what they look like in very practical terms. Our aim, therefore, is to perform a case study of magic production at colliders, using top pairs in the Standard Model as an illustrative example. We fully expect our results to generalise beyond this, and hope that our results prove useful in the ongoing discussions taking place between two different subfields of physics.

The structure of our paper is as follows. In section 2, we review concepts from quantum computing / information theory, including the notion of magic. In section 3, we classify in detail how magic is manifested in top pair production at the LHC. We discuss our results and conclude in section 4.

## 2 Review of relevant concepts

In this section, we will review salient details of quantum computing and magic. Given the wider than usual potential audience of this paper, we aim to be introductory and self-contained, as well as to set up conventions that will be needed throughout. The basic ingredient of the classical computer is the *bit*, that may assume the binary values 0 and 1. The simplest quantum computers replace this notion with a *qubit*, namely an individual quantum two-state system whose general state  $|\psi\rangle$  is a superposition of two orthogonal basis states  $|0\rangle$  and  $|1\rangle$ :

$$|\psi\rangle = \alpha|0\rangle + \beta|1\rangle. \quad (1)$$

Here  $\alpha$  and  $\beta$  are complex numbers satisfying the normalisation condition

$$|\alpha|^2 + |\beta|^2 = 1, \quad (2)$$

and such that the probability of measuring the qubit in the state  $|0\rangle$  or  $|1\rangle$  is given by  $|\alpha|^2$  or  $|\beta|^2$  respectively. A general quantum circuit then takes a number of qubits, and subjects them to a series of transformations, each of which may act on single or multiple qubits. In order to conserve probability, these transformations should be unitary, and each such transformation is referred to as a *quantum gate*, given that this mimics the action of logic gates on bits in classical computing. A universal quantum computer is one which has a sufficient number and variety of quantum gates, such that it can reproduce the effect of an arbitrary multi-qubit unitary transformation.

There are various ways to represent the effect of quantum gates. First, let us consider gates that act on a single qubit individually. The general state of the qubit can be written in column form as

$$|\psi\rangle = \begin{pmatrix} \alpha \\ \beta \end{pmatrix}, \quad (3)$$

using the basis states appearing in eq. (1). The action of a single-qubit gate will then be a  $2 \times 2$  matrix, and examples include the *phase gate*

$$P(\phi) = \begin{pmatrix} 1 & 0 \\ 0 & i \end{pmatrix} \quad (4)$$

(so-called because it introduces a  $\pi/2$  phase shift  $\phi$  between the basis states  $|0\rangle$  and  $|1\rangle$ ), and the *Hadamard gate*

$$H = \frac{1}{\sqrt{2}} \begin{pmatrix} 1 & 1 \\ 1 & -1 \end{pmatrix}, \quad (5)$$

which is widely used in quantum circuits. For multi-qubit gates, let us first note that a general  $n$ -qubit state will be a superposition of basis states

$$|\alpha_1\alpha_2\dots\alpha_n\rangle \equiv |\alpha_1\rangle \otimes |\alpha_2\rangle \otimes \dots \otimes |\alpha_n\rangle, \quad (6)$$

where  $\alpha_i \in \{0, 1\}$ . The number of individual basis states will be  $2^n$ , given that each individual qubit has two independent states. One way to specify the action of a multi-qubit gate is then to choose some ordering of these basis states, and to represent the action of a gate as a matrix. As an example, consider the 2-qubit system with basis states ( $|00\rangle, |01\rangle, |10\rangle, |11\rangle$ ). A general 2-qubit

gate will be representable as a  $4 \times 4$  unitary matrix, and a particular example that is heavily used in quantum computing is the *controlled NOT (CNOT) gate*, whose associated matrix is

$$\text{CNOT} = \begin{pmatrix} 1 & 0 & 0 & 0 \\ 0 & 1 & 0 & 0 \\ 0 & 0 & 0 & 1 \\ 0 & 0 & 1 & 0 \end{pmatrix}. \quad (7)$$

A special class of quantum gates consists of those that act independently on individual qubits. One may write such gates in tensor product notation as

$$U = U_1 \otimes U_2 \otimes \dots \otimes U_n, \quad (8)$$

where the action of the gate on a multiqubit state is

$$U \left[ |\alpha_1\rangle \otimes |\alpha_2\rangle \otimes \dots \otimes |\alpha_n\rangle \right] = (U_1|\alpha_1\rangle) \otimes (U_2|\alpha_2\rangle) \otimes \dots \otimes (U_n|\alpha_n\rangle). \quad (9)$$

Quantum computers differ from their classical counterparts due to the two key phenomena of *superposition* and *entanglement*. The former is already seen in eq. (1), and implies that we can view a multi-qubit quantum computation (before measurement) as a superposition of a large number of possible classical computations. Likewise, the creation of entangled states of qubits has no classical counterpart, and the presence of entanglement in certain well-known quantum algorithms allows for an exponential speed-up relative to classical computing [33, 34]. Despite this, the naïve expectation that entanglement is sufficient to yield powerful speed-ups over classical computing is not in fact true. For any number of qubits, there is a certain number of so-called *stabiliser states*, which include some maximally entangled configurations, and whose precise definition will be given below. The *Gottesman-Knill theorem* [35] states that quantum circuits involving stabiliser states only can be efficiently simulated using a classical computer. Put more simply, entanglement by itself is not enough to provide an advantage over classical algorithms, and something else is therefore needed in order to fully realise quantum perks. One can then introduce a property that measures “non-stabiliserness” of a multi-qubit state, and this property is known as *magic* in the quantum computing literature. Various definitions have been given to quantify this effect, and the concept of magic plays a key role in designing fault-tolerant computational algorithms. Here, we have been inspired by ref. [36], which looks at how to increase magic in larger multi-qubit systems.

Let us now explore the notions of stabiliser circuits and magic in more detail. Given a (multi-qubit) quantum state  $|\psi\rangle$ , we say that it is *stabilised* by a unitary operator  $U$  provided

$$U|\psi\rangle = |\psi\rangle. \quad (10)$$

A particular class of quantum states has been well-studied for various reasons, namely those that are stabilised by elements of the *Pauli group*. For a single qubit, this group is defined via the set of matrices

$$G_1 = \{\pm I, \pm iI, \pm\sigma_1, \pm i\sigma_1, \pm\sigma_2, \pm i\sigma_2, \pm\sigma_3, \pm i\sigma_3\}. \quad (11)$$

Here  $I$  is the  $2 \times 2$  identity matrix, and  $(\sigma_1, \sigma_2, \sigma_3)$  are the Pauli matrices:

$$\sigma_1 = \begin{pmatrix} 0 & 1 \\ 1 & 0 \end{pmatrix}, \quad \sigma_2 = \begin{pmatrix} 0 & -i \\ i & 0 \end{pmatrix}, \quad \sigma_3 = \begin{pmatrix} 1 & 0 \\ 0 & -1 \end{pmatrix}. \quad (12)$$

One may verify that multiplication of any two elements from eq. (11) gives another element of the group, so that this is indeed closed as required. More generally, one may define the  $n$ -qubit Pauli group  $G_n$

$$G_n = \{A_1 \otimes A_2 \otimes \dots \otimes A_n; A_i \in G_1\}. \quad (13)$$

In words, the elements of  $G_n$  consist of tensor products of operators  $A_i$  from the one-qubit Pauli group, each acting on a single qubit  $i$ . Let us define a general *Pauli string* as an operator

$$\mathcal{P}_n = P_1 \otimes P_2 \otimes \dots \otimes P_N, \quad P_a \in \{\sigma_1^{(a)}, \sigma_2^{(a)}, \sigma_3^{(a)}, I^{(a)}\}, \quad (14)$$

where e.g.  $\sigma^{(a)}$  and  $I^{(a)}$  are Pauli and identity matrices acting on qubit  $a$ . The elements of the  $n$ -qubit Pauli group are then given by Pauli strings weighted by factors  $\pm 1, \pm i$ .

The importance of these definitions for quantum computing stems from the following results (see e.g. Theorem 1 in ref. [37]). Imagine preparing an  $n$ -qubit quantum circuit with initial state

$$|0\rangle^{\otimes n} \equiv |0\rangle \otimes |0\rangle \otimes \dots \otimes |0\rangle. \quad (15)$$

Now consider that our quantum circuit only contains CNOT, Hadamard and phase gates. One may then show that  $|\psi\rangle$  is stabilised by exactly  $2^n$  Pauli strings (up to factors  $\pm 1$ ). Such circuits are called *stabiliser circuits*, and the resulting states are called *stabiliser states*. One may further prove (again see ref. [37]) that the number of independent stabiliser states for  $n$  qubits is

$$N = 2^n \prod_{k=0}^{n-1} (2^{n-k} + 1). \quad (16)$$

As an example, this predicts six stabiliser states for a single qubit system. These can be found by acting on  $|0\rangle$  and  $|1\rangle$  repeatedly with Hadamard and phase gates, yielding the six states

$$|0\rangle, \quad \frac{1}{\sqrt{2}} (|0\rangle \pm |1\rangle), \quad \frac{1}{\sqrt{2}} (|0\rangle \pm i|1\rangle), \quad |1\rangle. \quad (17)$$

From above, we expect each of these states to be an eigenstate of two operators chosen from  $(I, \sigma_1, \sigma_2, \sigma_3)$ , where these two operators could be different for each state. As an example,  $|0\rangle$  is an eigenstate of  $I$  and  $\sigma_3$  with eigenvalue 1 in both cases (and is not an eigenstate of  $\sigma_1$  or  $\sigma_2$ ). The state  $(|0\rangle + i|1\rangle)/\sqrt{2}$  is an eigenstate of  $I$  and  $\sigma_2$ , with eigenvalue 1. Similar conclusions can be reached for the other states.

Armed with the concepts of stabiliser circuits and states, we can now describe the Gottesman-Knill theorem more precisely (see also section 10.5.4 of ref. [2]). This states that there is an efficient classical algorithm to simulate any quantum circuit that: (i) starts with a state prepared in the computational basis; (ii) contains only Hadamard, phase, CNOT and Pauli gates (i.e. where the latter implement action of the Pauli matrices on a single qubit); (iii) involves measurements of observables in the Pauli group; (iv) may contain additional classical manipulation of the output. In pedestrian terms, this means that stabiliser circuits provide no genuine computational advantage over classical circuits, despite the fact that they may contain maximally entangled states. The presence of the latter can be clearly seen in eq. (17), in which four of the states are maximally entangled, i.e. consisting of a superposition of the form of eq. (1) with  $|\alpha| = |\beta|$ .

If superposition and entanglement by themselves are not enough to guarantee powerful quantum computers, there must be some other property of quantum states that is relevant. This property is

referred to as *magic* in the quantum computing literature, and various proposals have been given regarding how to quantify it [22–32]. By definition, stabiliser states have zero magic, and thus one needs to write down quantities which indeed give zero for stabiliser states, but give some non-zero measure of “non-stabiliserness” for general states. Here, we will follow the presentation of ref. [32], which starts with the above observation that  $n$ -qubit stabiliser states are such that the eigenvalues of  $2^n$  Pauli strings are straightforward (i.e.  $\pm 1$ ), whereas the others are zero. This suggests that, for a general state  $|\psi\rangle$ , we can consider its *Pauli spectrum*

$$\text{spec}(|\psi\rangle) = \{\langle\psi|P|\psi\rangle, \quad P \in \mathcal{P}_n\}. \quad (18)$$

That is, the Pauli spectrum of  $|\psi\rangle$  is a list of expectation values of each individual Pauli string in eq. (14), evaluated in the state  $|\psi\rangle$ . For a stabiliser state, this is a list containing mostly zero values, with  $2^n$  non-zero values  $\pm 1$ . For magic states, a more non-trivial pattern is obtained. From the Pauli spectrum, one may define something called the *stabiliser Rényi entropies (SREs)*, first defined in ref. [38], and consisting of the following family of functions  $\{M_q\}$  defined by integer values  $q \geq 2$ :

$$M_q = \frac{1}{1-q} \log_2(\zeta_q), \quad \zeta_q \equiv \sum_{P \in \mathcal{P}_n} \frac{\langle\psi|P|\psi\rangle^{2q}}{2^n}. \quad (19)$$

We can see that each  $M_q$  function involves a sum over expectation values of the Pauli strings, raised to powers. As argued in ref. [38] (see also ref. [32]), the set of values  $\{M_q\}$  measures the spread of the Pauli spectrum for general states, viewed as a distribution. Note that for a stabiliser state,  $M_q = 0$  for all  $q$ . To see this, recall that the expectation value of  $2^n$  of the possible Pauli strings is  $\pm 1$  for a stabiliser state  $|\psi\rangle$ , and zero for all of the other Pauli strings. Thus,  $\zeta_q = 1$  for stabiliser states, and  $M_q = \log_2(1)/(1-q) = 0$ . Below, we will take the case  $q = 2$  as a representative measure of magic, for which  $M_2$  is known as the *Second Stabiliser Rényi entropy (SSRE)*.

### 3 Are top quarks magic?

#### 3.1 Results for partonic initial states

Let us now turn to the question of whether magic can be probed in collider physics. To this end, we will consider a well-studied system from the point of view of entanglement, namely the production of a top-antitop pair at the LHC. Given that top quarks are spin-1/2 particles, this constitutes a naturally produced two-qubit system. At leading order in the Standard Model, top quark pair production proceeds via the strong interaction, and there are two partonic channels as shown in figure 1. In each case, QFT predicts the possible states of the top quarks (e.g. their momenta, spins and energies). The top quarks will not be in a uniquely predicted state, but instead must be regarded as in a statistical mixture of possible states, with associated probabilities. There is a well-developed formalism for dealing with such situations in quantum theories, known as the *density matrix formalism*. To introduce this in general, consider a quantum system that can be in any one of a number of states  $|\psi_i\rangle$ , each with probability  $p_i$ . One may then define the *density matrix*

$$\rho = \sum_i p_i |\psi_i\rangle\langle\psi_i|, \quad (20)$$

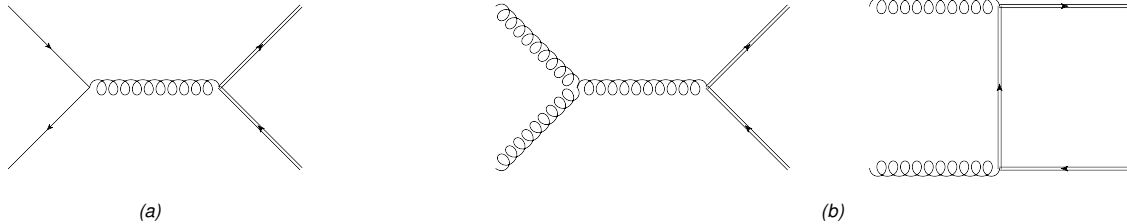


Figure 1: LO Feynman diagrams for top-antitop pair production in the SM, where a double line represents a top particle: (a)  $q\bar{q}$  channel; (b)  $gg$  channel. The two channels contribute roughly 10% and 90% of the total cross-section respectively.

where the probabilities must necessarily satisfy

$$p_i \geq 0, \quad \sum_i p_i = 1. \quad (21)$$

If a given system is found to be in a single overall state  $|\psi\rangle$  (with unit probability), its density matrix has the special form

$$\rho = |\psi\rangle\langle\psi|, \quad (22)$$

and the system is said to be in a *pure state*. If instead two or more probabilities in eq. (20) are non-zero, then the system is said to be in a *mixed state*. As stated above, it is this latter case that will apply to top quarks produced by a collider experiment, as the rules of QFT give us at most the identity of each possible final state, and its associated probability. Faced with such an ensemble of possible final states, the expectation value of an observable  $\mathcal{O}$  will be given by

$$\langle\mathcal{O}\rangle = \sum_i p_i \langle\psi_i|\mathcal{O}|\psi_i\rangle = \text{Tr}[\rho\mathcal{O}], \quad (23)$$

where the second line recognises that this is the trace of the density matrix multiplied by the operator in matrix form.

The language of density matrices is used heavily in the context of entanglement, due to the ease of defining clear criteria for states to be entangled. Considering two subsystems  $A$  and  $B$  of a larger whole, the density matrix  $\rho$  is *separable* if it can be written in the form

$$\rho = \sum_i p_i \rho_i^A \otimes \rho_i^B. \quad (24)$$

Separable states contain no quantum entanglement between the subsystems  $A$  and  $B$ . Similarly, entangled states cannot be written in a separable form. This in turn allows various algebraic criteria for entanglement to be obtained (see e.g. refs. [3, 4, 21] for a review), which in turn have guided experimental searches for top quark entanglement. In such analyses, it is entanglement of the (anti-)top quark spins that is being talked about, and there will be a density matrix describing the (in general mixed) state of a top-antitop pair. The definition of this can be found in e.g. ref. [4], and there are different levels at which one can define it. First, let us note that the kinematics of a pair of top particles in the centre of mass frame will be specified by their invariant mass  $M$ , the unit direction vector  $\mathbf{k}$  of one of the particles, and the spins  $\alpha$  and  $\beta$  of each particle. These

quantities can be used to specify a complete set of possible final states  $|M\hat{\mathbf{k}}\alpha\beta\rangle$ . If we then let  $|I\lambda\rangle$  denote a given initial state  $I$  (with associated quantum numbers  $\lambda$ ), then the quantum (scattering) amplitude for proceeding from this initial state to one of the possible final states is, by definition,

$$\mathcal{A}_{\alpha\beta}^\lambda = \langle M\hat{\mathbf{k}}\alpha\beta|\hat{T}|I\lambda\rangle \quad (25)$$

where  $\hat{T}$  is the *transition operator*. We can then define the so-called  $R$ -matrix

$$R_{\alpha\beta,\alpha'\beta'}^{I\lambda}(M, \hat{\mathbf{k}}) = \mathcal{A}_{\alpha\beta}^\lambda(M, \hat{\mathbf{k}}) \left[ \mathcal{A}_{\alpha'\beta'}^\lambda(M, \hat{\mathbf{k}}) \right]^\dagger. \quad (26)$$

This is like a squared amplitude that enters a cross-section, except for the fact that the final states are different, and thus the spin indices will not be contracted. In a collider experiment, we do not usually have control over the precise initial states, which must therefore be averaged over initial quantum numbers (e.g. colours, spins etc.). Thus, we can define the averaged  $R$ -matrix:

$$R_{\alpha\beta,\alpha'\beta'}^I(M, \hat{\mathbf{k}}) = \frac{1}{N_\lambda} \sum_\lambda R_{\alpha\beta,\alpha'\beta'}^{I\lambda}(M, \hat{\mathbf{k}}). \quad (27)$$

This is sometimes loosely referred to as the *production (spin) density matrix*, but strictly speaking this should be normalised to have unit trace:

$$\rho^I = \frac{R^I}{\text{Tr}(R^I)}. \quad (28)$$

This is not the only density matrix we can talk about to describe the top quark final state. We might also wish to describe the top quark mixed state that results after we sum over all possible final states with a given invariant mass (i.e. summing over all possible top quark directions). The resulting density matrix is given by [4]

$$\bar{\rho}^I(M) = \frac{1}{Z} \sum_{\alpha\beta,\alpha'\beta'} \int d\Omega R_{\alpha\beta,\alpha'\beta'}^I(M, \hat{\mathbf{k}}) \frac{|M\hat{\mathbf{k}}\alpha\beta\rangle\langle M\hat{\mathbf{k}}\alpha'\beta'|}{\langle M\hat{\mathbf{k}}|M\hat{\mathbf{k}}\rangle}. \quad (29)$$

Here, the denominator of the integrand normalises the final states, which are then weighted with the production density matrix. There is then an integral over all possible solid angles (i.e. over the top quark directions), and the overall prefactor contains a normalisation factor  $Z$ .

Let us focus on the production density matrix  $R^I$ , which is fully differential in the final state kinematics. This quantity specifies a general mixed state of the top-antitop pair, and will depend upon the invariant mass of the latter, and the directions of the top particles in general. This is what we expect of course: QFT tells us that the probability of producing a given final state depends upon its kinematics. The “mixed” top quark final state constitutes a superposition of the possible final states for each point in the kinematic phase space, weighted by the appropriate probabilities as predicted by QFT. Results for the top quark production density matrix, for the initial states  $I = q\bar{q}, gg$ , can be found e.g. in ref. [4]. The first step in presenting this is to note that a two-qubit  $R$ -matrix has the general decomposition

$$R^I = \tilde{A}^I I_4 + \sum_i \left( \tilde{B}_i^{I+} \sigma_i \otimes I_2 + \tilde{B}_i^{I-} I_2 \otimes \sigma_i + \sum_{i,j} \tilde{C}_{ij}^I \sigma_i \otimes \sigma_j \right). \quad (30)$$

Here  $I_n$  denotes an  $n$ -dimensional identity matrix, and  $\sigma_i$  a Pauli matrix. The kinematic dependence of the  $R$ -matrix is then sitting in the various coefficients  $\{\tilde{A}^I, \tilde{B}_i^{I\pm}, \tilde{C}_{ij}^I\}$ . Upon taking the trace of eq. (30), only the first term survives, such that the normalised production density matrix is given by

$$\rho^I = \frac{R^I}{4\tilde{A}^I}. \quad (31)$$

We can then use a similar decomposition to eq. (30) for the normalised density matrix, with coefficients

$$B_i^{I\pm} = \frac{\tilde{B}_i^{I\pm}}{\tilde{A}^I}, \quad C_{ij}^I = \frac{\tilde{C}_{ij}^I}{\tilde{A}^I}. \quad (32)$$

To give explicit forms for the coefficients, we need to choose a convenient coordinate system, and a common choice is the so-called *helicity basis* [39], illustrated in figure 2. This introduces two vectors  $\hat{n}$  and  $\hat{r}$  transverse to the top quark direction, which can be formally defined as follows:

$$\hat{r} = \frac{\hat{\mathbf{p}} - \cos\theta \hat{\mathbf{k}}}{\sin(\theta)}, \quad \hat{n} = \hat{r} \times \hat{\mathbf{k}}, \quad (33)$$

where  $\hat{\mathbf{p}}$  is the direction of the first incoming beam, and  $\cos\theta = \hat{\mathbf{k}} \cdot \hat{\mathbf{p}}$  defines the scattering angle. As noted in ref. [4], a particular advantage of the helicity basis is that a boost along the top quark direction does not change its orientation. Thus, spin information defined in the rest frame of each top particle is easily relatable to the centre of mass frame in which the top quarks are measured. One may furthermore show that the following relations hold at LO in the SM:

$$\tilde{B}_i^{I+} = \tilde{B}_i^{I-} = 0, \quad \tilde{C}_{ij}^I = \tilde{C}_{ji}^I, \quad (34)$$

also that certain coefficients in the helicity basis vanish:

$$\tilde{C}_{nr}^I = \tilde{C}_{nk}^I = 0. \quad (35)$$

The remaining non-zero coefficients will be functions of the top quark invariant mass and scattering angle. Rather than the former, it is conventional to introduce the variable

$$\beta = \sqrt{1 - \frac{4m_t^2}{M}}, \quad (36)$$

which can be shown to be the velocity of the top quark (in natural units), with  $m_t$  the top quark mass. We can see that this makes sense from eq. (36):  $\beta = 0$  or  $1$  at threshold ( $M = 2m_t$ ) or high energy respectively, where the top quark velocity in the latter case approaches the speed of light. Defining also

$$z = \cos\theta, \quad (37)$$

we may quote for the non-zero  $R$ -matrix coefficients at LO in the SM from ref. [5]. For the  $q\bar{q}$  and  $gg$  channels respectively one has

$$\begin{aligned} \tilde{A}^{q\bar{q}} &= F_{q\bar{q}} \left( 2 + \beta^2(z^2 - 1) \right); \\ \tilde{C}_{nn}^{q\bar{q}} &= F_{q\bar{q}} \beta^2(z^2 - 1); \\ \tilde{C}_{kk}^{q\bar{q}} &= F_{q\bar{q}} \left( \beta^2 + z^2(2 - \beta^2) \right); \end{aligned}$$

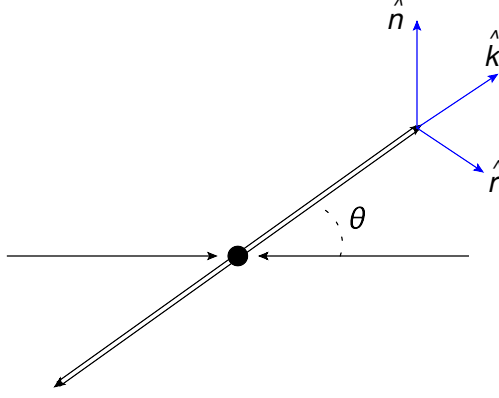


Figure 2: Illustration of the helicity basis, used to define the coefficients of the top quark production density matrix. The single and double arrows represent the incoming beams and outgoing top quark directions respectively, with  $\theta$  the scattering angle. The top quark direction is given by the unit vector  $\hat{\mathbf{k}}$ , where  $\hat{\mathbf{n}}$  and  $\mathbf{r}$  are defined in the plane transverse to this.

$$\begin{aligned}\tilde{C}_{rr}^{q\bar{q}} &= F_{q\bar{q}}\left(2 - \beta^2 - z^2(2 - \beta^2)\right); \\ \tilde{C}_{rk}^{q\bar{q}} &= 2zF_{q\bar{q}}\sqrt{(1 - z^2)(1 - \beta^2)};\end{aligned}\quad (38)$$

and

$$\begin{aligned}\tilde{A}^{gg} &= F_{gg}\left(1 + 2\beta^2(1 - z^2) - \beta^4(z^4 - 2z^2 + 2)\right); \\ \tilde{C}_{nn}^{gg} &= -F_{gg}\left(1 - 2\beta^2 + \beta^4(z^4 - 2z^2 + 2)\right); \\ \tilde{C}_{kk}^{gg} &= -F_{gg}\left(1 - 2z^2(1 - z^2)\beta^2 - (2 - 2z^2 + z^4)\beta^4\right); \\ \tilde{C}_{rr}^{gg} &= -F_{gg}\left(1 - (2 - 2z^2 + z^4)\beta^2(2 - \beta^2)\right); \\ \tilde{C}_{rk}^{gg} &= 2zF_{gg}(1 - z^2)^{3/2}\beta^2\sqrt{1 - \beta^2};\end{aligned}\quad (39)$$

where

$$F_{q\bar{q}} = \frac{1}{18}, \quad F_{gg} = \frac{7 + 9\beta^2 z^2}{192(1 - \beta^2 z^2)^2}.\quad (40)$$

Using these results, one may evaluate the magic of a top-antitop pair, for different partonic channels and / or kinematics. To do so, we must first note that the definition of the SSRE  $M_2$  given in eq. (19) is for pure states, whereas we are instead dealing with a mixed state. One may, however, generalise the above notions to this context. First, as discussed in ref. [38] (see in particular the supplementary material), an  $n$ -qubit mixed stabiliser state is defined by having a density matrix of the form

$$\rho = \frac{1}{2^n} \left( I_4 + \sum_{P \in G} \phi_P P \right).\quad (41)$$

Here  $P$  is a Pauli string;  $G$  a subset of the  $n$ -qubit Pauli group with  $0 < |G| < d - 1$  elements; and  $\phi_P = \pm 1$  for each  $P$ . Such a state has a Pauli spectrum containing trivial values  $\pm 1$ , and thus is

a natural generalisation of the concept of a pure stabiliser state. It turns out also that there is a simple tweak of the definition of  $M_2$  such that this is zero for mixed stabiliser states. First, let us note that the pure state definition of  $M_q$  of eq. (19) contains the quantity

$$\langle \psi | P | \psi \rangle = \text{Tr}(P\rho), \quad (42)$$

where  $P$  is a Pauli string, and  $\rho$  the density matrix corresponding to the (pure) state  $|\psi\rangle$ . The formula for  $M_2$  can then be written as

$$M_2(\rho) = -\log_2 \left( \frac{\sum_{P \in \mathcal{P}_n} \text{Tr}^4(\rho P)}{2^n} \right). \quad (43)$$

The appropriate modification of this for mixed states is [38]

$$\tilde{M}_2(\rho) = -\log_2 \left( \frac{\sum_{P \in \mathcal{P}_n} \text{Tr}^4(\rho P)}{\sum_{P \in \mathcal{P}_n} \text{Tr}^2(\rho P)} \right), \quad (44)$$

and plugging in the decomposition of eqs. (30, 31) eventually gives

$$\tilde{M}_2(\rho^I) = -\log_2 \left( \frac{(\tilde{A}^I)^4 + (\tilde{C}_{nn}^I)^4 + (\tilde{C}_{kk}^I)^4 + (\tilde{C}_{rr}^I)^4 + 2(\tilde{C}_{rk}^I)^4}{(\tilde{A}^I)^2[(\tilde{A}^I)^2 + (\tilde{C}_{nn}^I)^2 + (\tilde{C}_{kk}^I)^2 + (\tilde{C}_{rr}^I)^2 + 2(\tilde{C}_{rk}^I)^2]} \right). \quad (45)$$

Using eqs. (38, 39), we can now plot the amount of magic in a top-antitop pair, as measured by  $\tilde{M}_2$ , and as predicted by the SM at LO. Results are shown in the  $(z, \beta)$  plane in figure 3, where we have used a top quark mass of  $m_t = 172.76\text{GeV}$ . There are a number of notable features. First, it is relatively generic that magic top quark states are produced throughout most of phase space. There are then several regions or limits in which the magic vanishes completely. This can be related to known results in the literature [4], as we discuss in the following section.

### 3.2 When has the magic gone?

In order to analyse where the SSRE is zero, it will be useful to find the form of the  $R$ -matrix in different kinematic limits. Following ref. [4], one may then relate it to specific quantum states, which gives further physical insight into why magic vanishes. We can write each of the operators in eq. (30) in terms of an explicit  $4 \times 4$  matrix acting on the computational basis ( $|00\rangle, |01\rangle, |10\rangle, |11\rangle$ ), where for each particle  $|0\rangle$  and  $|1\rangle$  represent a spin up or down state in the  $\mathbf{k}$  direction respectively. In terms of the coordinate basis of figure 2, this means that we define Pauli matrices

$$\sigma_n = \sigma_1, \quad \sigma_r = \sigma_2, \quad \sigma_k = \sigma_3. \quad (46)$$

In other words, the (1,2,3) directions in spin space (represented by the Pauli matrices of eq. (12)) are mapped to the  $(\mathbf{n}, \mathbf{r}, \mathbf{k})$  directions respectively, which then constitute a right-handed coordinate system. Consider then the example operator  $\sigma_n \otimes \sigma_n$ . An explicit computation gives

$$\begin{aligned} \sigma_n \otimes \sigma_n |00\rangle &= [\sigma_n |0\rangle] \otimes [\sigma_n |0\rangle] \\ &= \left[ \begin{pmatrix} 0 & 1 \\ 1 & 0 \end{pmatrix} \begin{pmatrix} 1 \\ 0 \end{pmatrix} \right] \otimes \left[ \begin{pmatrix} 0 & 1 \\ 1 & 0 \end{pmatrix} \begin{pmatrix} 1 \\ 0 \end{pmatrix} \right] \end{aligned}$$

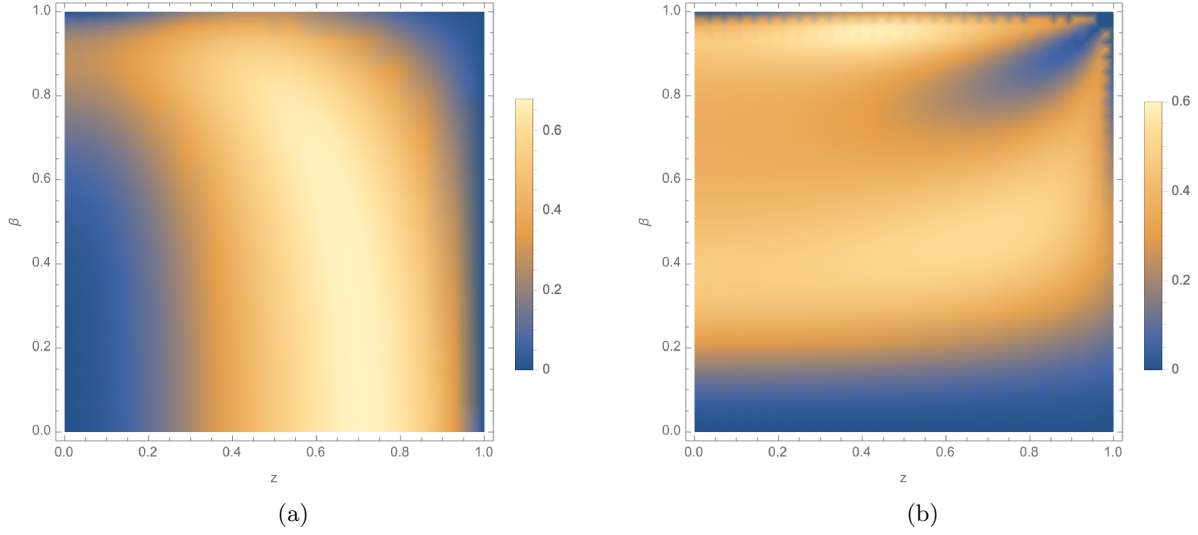


Figure 3: The magic of a mixed top-antitop final state in: (a) the  $q\bar{q}$  channel; (b) the  $gg$  channel.

$$\begin{aligned}
&= \left[ \begin{pmatrix} 0 \\ 1 \end{pmatrix} \right] \otimes \left[ \begin{pmatrix} 0 \\ 1 \end{pmatrix} \right] \\
&= |11\rangle.
\end{aligned} \tag{47}$$

Likewise, we find

$$\sigma_n \otimes \sigma_n |01\rangle = |10\rangle, \quad \sigma_n \otimes \sigma_n |10\rangle = |01\rangle, \quad \sigma_n \otimes \sigma_n |11\rangle = |00\rangle, \tag{48}$$

such that the matrix form of the operator in the computational basis is

$$\sigma_n \otimes \sigma_n = \begin{pmatrix} 0 & 0 & 0 & 1 \\ 0 & 0 & 1 & 0 \\ 0 & 1 & 0 & 0 \\ 1 & 0 & 0 & 0 \end{pmatrix}. \tag{49}$$

Using similar methods, one finds the following:

$$\begin{aligned}
\sigma_k \otimes \sigma_k &= \begin{pmatrix} 1 & 0 & 0 & 0 \\ 0 & -1 & 0 & 0 \\ 0 & 0 & -1 & 0 \\ 0 & 0 & 0 & 1 \end{pmatrix}, & \sigma_r \otimes \sigma_r &= \begin{pmatrix} 0 & 0 & 0 & -1 \\ 0 & 0 & 1 & 0 \\ 0 & 1 & 0 & 0 \\ -1 & 0 & 0 & 0 \end{pmatrix}, \\
\sigma_r \otimes \sigma_k &= \begin{pmatrix} 0 & 0 & i & 0 \\ 0 & 0 & 0 & -i \\ -i & 0 & 0 & 0 \\ 0 & i & 0 & 0 \end{pmatrix}, & \sigma_k \otimes \sigma_r &= \begin{pmatrix} 0 & i & 0 & 0 \\ -i & 0 & 0 & 0 \\ 0 & 0 & 0 & -i \\ 0 & 0 & i & 0 \end{pmatrix}.
\end{aligned} \tag{50}$$

Due to the fact that only certain coefficients in eq. (30) are non-vanishing at LO in the SM, one has the simplified decomposition

$$R^I(z, \beta) = \tilde{A}^I I_4 + \tilde{C}_{nn}^I \sigma_n \otimes \sigma_n + \tilde{C}_{rr}^I \sigma_r \otimes \sigma_r + \tilde{C}_{kk}^I \sigma_k \otimes \sigma_k + \tilde{C}_{rk}^I (\sigma_r \otimes \sigma_k + \sigma_k \otimes \sigma_r), \tag{51}$$

where we have used the symmetry property of the  $\tilde{C}_{ij}^I$  coefficients noted in eq. (35). By plugging in the results of eqs. (39, 38), one then has a complete form for the  $R$ -matrix in the computational basis, with full kinematic dependence.

Now let us look at the regions in figure 3 where the magic vanishes, and see what happens to the  $R$ -matrix in each case. For the  $q\bar{q}$  channel, these limits give

$$R^{q\bar{q}}(1, \beta) \propto \begin{pmatrix} 1 & 0 & 0 & 0 \\ 0 & 0 & 0 & 0 \\ 0 & 0 & 0 & 0 \\ 0 & 0 & 0 & 1 \end{pmatrix}, \quad R^{q\bar{q}}(0, 1) \propto \begin{pmatrix} 1 & 0 & 0 & -1 \\ 0 & 0 & 0 & 0 \\ 0 & 0 & 0 & 0 \\ -1 & 0 & 0 & 1 \end{pmatrix}, \quad R^{q\bar{q}}(0, 0) \propto \begin{pmatrix} 1 & 0 & 0 & -1 \\ 0 & 1 & 1 & 0 \\ 0 & 1 & 1 & 0 \\ -1 & 0 & 0 & 1 \end{pmatrix}. \quad (52)$$

One may show that each of these matrices indeed meets the definition of stabiliserness given in eq. (41), in that each matrix can be written as a suitable linear combination of Pauli strings, with coefficients normalised appropriately. To gain further insight into what is happening to the top quarks in each limit, we may start with the first matrix in eq. (52), and note that this is equal to

$$\begin{pmatrix} 1 \\ 0 \\ 0 \\ 0 \end{pmatrix} (1 \ 0 \ 0 \ 0) + \begin{pmatrix} 0 \\ 0 \\ 0 \\ 1 \end{pmatrix} (0 \ 0 \ 0 \ 1), \quad (53)$$

which when translated into state notation yields

$$R^{q\bar{q}}(1, \beta) \propto |00\rangle\langle 00| + |11\rangle\langle 11|. \quad (54)$$

The density matrix is given by normalising this to have unit trace:

$$\rho^{q\bar{q}}(1, \beta) = \frac{|00\rangle\langle 00| + |11\rangle\langle 11|}{2}. \quad (55)$$

This agrees with eq. (26) of ref. [3], where that reference quotes the result as

$$\frac{|\uparrow_{\hat{p}}\uparrow_{\hat{p}}\rangle\langle\uparrow_{\hat{p}}\uparrow_{\hat{p}}| + |\downarrow_{\hat{p}}\downarrow_{\hat{p}}\rangle\langle\downarrow_{\hat{p}}\downarrow_{\hat{p}}|}{2}, \quad (56)$$

where  $|\uparrow_{\hat{p}}\rangle$  and  $|\downarrow_{\hat{p}}\rangle$  denote spin up and down states along the beam direction. That this is equivalent to eq. (55) follows from the fact that, if the scattering angle is  $0^\circ$  so that  $z = \cos(\theta) = 1$ , then the top quark direction  $\hat{\mathbf{k}}$  is the same as the beam direction  $\hat{\mathbf{p}}$ .

It is also possible to describe the other  $R$ -matrices in eq. (52) in terms of specific states. For the second, and inspired by refs. [3, 5], let us define the single qubit states

$$|\uparrow_{\hat{n}}\rangle = \frac{|0\rangle + |1\rangle}{\sqrt{2}}, \quad |\downarrow_{\hat{n}}\rangle = \frac{|0\rangle - |1\rangle}{\sqrt{2}}, \quad (57)$$

which constitute spin up and down states in the  $\hat{\mathbf{n}}$  direction respectively<sup>3</sup>. Then, we can define the two-qubit states

$$|\Psi^\pm\rangle = \frac{|\uparrow_{\hat{n}}\downarrow_{\hat{n}}\rangle \pm |\downarrow_{\hat{n}}\uparrow_{\hat{n}}\rangle}{\sqrt{2}}, \quad (58)$$

---

<sup>3</sup>To see this, note that  $(1, 1)$  and  $(1, -1)$  are eigenstates of the Pauli matrix  $\sigma_n$  with eigenvalues  $\pm 1$ .

which substitution of eq. (57) reveals to be given in the computational basis by

$$|\Psi^+\rangle = \frac{|00\rangle - |11\rangle}{\sqrt{2}} \equiv \frac{1}{\sqrt{2}} \begin{pmatrix} 1 \\ 0 \\ 0 \\ -1 \end{pmatrix}, \quad |\Psi^-\rangle = \frac{|10\rangle - |01\rangle}{\sqrt{2}} \equiv \frac{1}{\sqrt{2}} \begin{pmatrix} 0 \\ -1 \\ 1 \\ 0 \end{pmatrix}. \quad (59)$$

The column vector form can be used to show that the normalised density matrix corresponding to the second  $R$ -matrix in eq. (52) is given by

$$\rho^{q\bar{q}}(0, 1) = |\Psi^+\rangle\langle\Psi^+|, \quad (60)$$

which agrees with eq. (24) of ref. [3]. Using similar techniques, the final matrix in eq. (52) can be shown to give rise to the density matrix

$$\rho^{q\bar{q}}(0, 0) = \frac{|\Psi^+\rangle\langle\Psi^+| + |\Psi_1\rangle\langle\Psi_1|}{\sqrt{2}}, \quad |\Psi_1\rangle = \frac{|01\rangle + |10\rangle}{\sqrt{2}}. \quad (61)$$

From eq. (60), we see that  $\rho^{q\bar{q}}(0, 1)$  describes a pure state. Furthermore, this is maximally entangled, as can be seen from the definition of  $|\Psi^+\rangle$  in eq. (58). It is in fact a known two-qubit stabiliser state, and corroborates the fact that maximal entanglement can be associated with vanishing magic. By contrast, eqs. (55, 61) constitute so-called *separable mixed states*, for which no quantum entanglement is present. Again the magic vanishes, so that the kinematic region of non-zero magic lies in between the two extremes of minimal and maximal entanglement.

Similar conclusions can be reached for the  $gg$  channel. In that case, the kinematic limits with vanishing magic, and their associated quantum states, are given by

$$\rho^{gg}(1, 1) = \frac{|00\rangle\langle 00| + |11\rangle\langle 11|}{2}, \quad \rho^{gg}(z, 0) = \frac{|\uparrow\hat{n}\downarrow\hat{n}\rangle - |\downarrow\hat{n}\uparrow\hat{n}\rangle}{\sqrt{2}}, \quad \rho^{gg}(0, 1) = |\Psi^+\rangle\langle\Psi^+|. \quad (62)$$

Again these are minimally and maximally entangled, with the region of non-zero magic lying in between.

### 3.3 Results for proton initial states

Above, we have presented results for individual partonic channels. However, the total top quark state produced at the LHC will be a weighted sum of partonic channels, taking into account the non-perturbative distributions of the quarks and gluons inside the colliding protons. As stated in ref. [3], it is straightforward to convert the individual partonic  $R$ -matrices of eq. (26) to their hadronic counterparts by forming the combination

$$R(M, \hat{\mathbf{k}}) = \sum_{I \in \{q\bar{q}, gg\}} L^I(M) R^I(M, \hat{\mathbf{k}}), \quad (63)$$

where we have introduced the parton luminosities

$$L^I(M) = \frac{1}{s} \frac{1}{1 + \delta_{ab}} \int_{\tau}^1 \frac{dx}{x} f_a(x, \sqrt{\hat{s}}) f_b\left(\frac{\tau}{x}, \sqrt{\hat{s}}\right) + (a \leftrightarrow b). \quad (64)$$

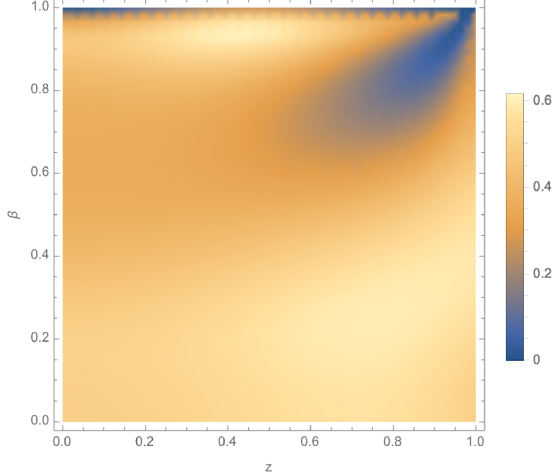


Figure 4: The magic of a mixed top-antitop final state at hadron level.

Here  $a$  and  $b$  are the two partons in partonic channel  $I$ ;  $f_a(x, Q)$  the parton distribution function with momentum fraction  $x$  and factorisation scale  $Q$ ; and  $\sqrt{\hat{s}}$  is the partonic centre of mass energy (equal to the top quark invariant mass  $M$  at LO). Finally,  $\tau$  is defined as

$$\tau = \frac{\hat{s}}{s}, \quad (65)$$

where  $\sqrt{s}$  is the hadronic centre of mass energy of 13TeV. Note that the definition of the luminosity in eq. (64) already symmetrises over the  $q\bar{q}$  and  $\bar{q}q$  channels, where the prefactor removes overcounting for the  $gg$  channel. From eq. (63), one may derive the normalised hadronic density matrix

$$\rho(M, \hat{\mathbf{k}}) = \sum_{I \in \{q\bar{q}, gg\}} w_I(M, \hat{\mathbf{k}}) \rho^I(M, \hat{\mathbf{k}}), \quad (66)$$

where  $\rho^I(M, \hat{\mathbf{k}})$  is the partonic density matrix of eq. (28), and we have followed ref. [3] in defining the parton weight functions

$$w_I(M, \hat{\mathbf{k}}) = \frac{L^I(M) \tilde{A}^I(M, \hat{\mathbf{k}})}{\sum_J L^J(M) \tilde{A}^J(M, \hat{\mathbf{k}})}. \quad (67)$$

In order to evaluate these expressions, we have used the publicly available `ManeParse` package for Mathematica [40]. Following ref. [5], we use the `NNPDF4.0` NNLO PDF set [41] with strong coupling constant  $\alpha_s(m_Z) = 0.118$ , and using the `LHAPDF` interface [42]. Results for the hadronic magic, analogous to the partonic results of figure 3, are shown in figure 4. Interestingly, we see that the magic still vanishes in the upper-right region of the plot, corresponding to high top invariant mass, and forward production. Such configurations correspond to the so-called *Regge limit*, in which the parton luminosity will be dominated by gluons. Indeed, the hadron-level plot in the upper-right region is extremely similar in structure to the purely gluonic result of figure 3(b).

Different behaviour is seen at low values of  $\beta$  and / or  $z$ , where none of the regions of low magic from figure 3(b) survive. Indeed, the magic no longer vanishes at  $(z, \beta) = 0$ , for which analytic

insight may be gained as follows. Let us first define the coefficients

$$C_{ij}^{\text{had.}}(z, \beta) = \frac{w_{q\bar{q}}(z, \beta)\tilde{C}_{ij}^{q\bar{q}}}{\tilde{A}^{q\bar{q}}} + \frac{w_{gg}(z, \beta)\tilde{C}_{ij}^{gg}}{\tilde{A}^{gg}}. \quad (68)$$

An explicit computation then shows that the hadron-level magic is given by

$$\tilde{M}_2^{\text{had.}}(\rho) = -\log_2 \left( \frac{1 + [C_{nn}^{\text{had.}}]^4 + [C_{kk}^{\text{had.}}]^4 + [C_{rr}^{\text{had.}}]^4 + 2[C_{rk}^{\text{had.}}]^4}{1 + [C_{nn}^{\text{had.}}]^2 + [C_{kk}^{\text{had.}}]^2 + [C_{rr}^{\text{had.}}]^2 + 2[C_{rk}^{\text{had.}}]^2} \right). \quad (69)$$

Using eqs. (39, 38, 40), one then finds

$$\tilde{M}_2^{\text{had.}} \Big|_{(z,\beta) \rightarrow (0,0)} = -\log_2 \left( \frac{2w_{gg}^4(0,0) + w_{q\bar{q}}^4(0,0) + 6w_{gg}^2(0,0)w_{q\bar{q}}^2(0,0)}{2w_{gg}^2(0,0)w_{q\bar{q}}^2(0,0)} \right). \quad (70)$$

Given that both  $w_{gg}(0,0)$  and  $w_{q\bar{q}}(0,0)$  are non-zero, eq. (70) will also return a non-zero result. The individual partonic cases correspond to  $w_{gg} \rightarrow 0$ ,  $w_{q\bar{q}} \rightarrow 1$  (or vice versa), in which case one recovers  $\tilde{M}_2 \rightarrow 0$  as expected. It may naively seem surprising that combining the partonic channels from figure 3(a) and (b) does not reproduce a feature that appears in both plots (i.e. the vanishing of the magic at  $(z, \beta) = (0, 0)$ ). However, it is important to recognise that, whilst the total hadronic density matrix is a simple weighted sum of the individual partonic channels, the same is not true for the magic. Indeed, there is a simple physical explanation for this behaviour: eqs. (61, 62) show that *different* stabiliser states occur in the  $(z, \beta) = (0, 0)$  limit for the  $gg$  and  $q\bar{q}$  channels. The fact that these are superposed with non-zero weights in the hadronic density matrix mean that the resulting state is non-stabiliser, and thus has non-zero magic. To see this in more detail, recall that the Pauli spectrum of a stabiliser state has entries  $\pm 1$  only. Adding together *different* stabiliser states with non-unit weights will therefore result in a Pauli spectrum containing non-unit values, which is necessarily non-stabiliser. We examine a further case of magic enhancement upon combining states in the following section.

### 3.4 Angular-averaged final states

So far, we have considered the magic of the top-antitop final state fully differentially in the kinematics (invariant mass and scattering angle). As stated in eq. (29), however, one may also wish to consider the top quark state after averaging over the top quark directions. To do this, one may consider a fixed spin basis, rather than the direction-dependent helicity basis. A common choice is the *beam basis*, in which the 3-direction in spin space is aligned with the first incoming beam direction (corresponding with the  $z$ -direction in Cartesian coordinates), and the 1- and 2-directions (corresponding with  $x$  and  $y$  directions in space) are chosen in the transverse plane so as to make a right-handed coordinate system. The partonic angular-averaged  $R$ -matrices will be given by expressions similar to eq. (30), and results for the various coefficients have been presented in ref. [3]. One finds that the  $\tilde{B}_i^{I\pm}$  coefficients vanish, and that the correlation matrix  $\tilde{C}_{ij}^I$  becomes diagonal:

$$\tilde{C}_{ij}^I = \begin{pmatrix} \tilde{C}_{\perp}^I & 0 & 0 \\ 0 & \tilde{C}_{\perp}^I & 0 \\ 0 & 0 & \tilde{C}_z^I \end{pmatrix}, \quad (71)$$

where we have adopted a common notation for the diagonal elements (n.b. the elements  $\tilde{C}_{xx}^I = \tilde{C}_{yy}^I \equiv \tilde{C}_{\perp}^I$  are equal). The non-zero coefficients are given by

$$\begin{aligned}\tilde{A}^{q\bar{q}}(M) &= \frac{1}{9} \left[ 1 - \frac{\beta^2}{3} \right]; \\ C_{\perp}^{q\bar{q}}(M) &= \frac{2}{135} f(\beta); \\ C_z^{q\bar{q}}(M) &= \frac{1}{9} \left[ 1 - \frac{\beta^2}{3} - \frac{4}{15} f(\beta) \right];\end{aligned}\tag{72}$$

and

$$\begin{aligned}\tilde{A}^{gg}(M) &= \frac{1}{192} \left[ -59 + 31\beta^2 + (66 - 36\beta^2 + 2\beta^4) \frac{\tanh^{-1}(\beta)}{\beta} \right]; \\ C_{\perp}^{gg}(M) &= \frac{1 - \beta^2}{192} \left[ 9 - \frac{16 \tanh^{-1}(\beta)}{\beta} \right] + g(\beta); \\ C_z^{gg}(M) &= \frac{1}{192} \left[ -109 + 49\beta^2 + (102 - 72\beta^2 + 2\beta^4) \frac{\tanh^{-1}(\beta)}{\beta} \right] - 2g(\beta)\end{aligned}\tag{73}$$

in the  $q\bar{q}$  and  $gg$  channels respectively, where we have followed ref. [3] in introducing the functions

$$\begin{aligned}f(\beta) &= \frac{(1 - \sqrt{1 - \beta^2})}{2}; \\ g(\beta) &= \frac{f(\beta)}{96\beta^4} \left[ 49 - \frac{149}{3}\beta^2 + \frac{24}{5}\beta^4 - (17\beta^4 - 66\beta^2 + 49) \frac{\tanh^{-1}(\beta)}{\beta} \right].\end{aligned}\tag{74}$$

Armed with these results, we can calculate the partonic angular-averaged magic using eq. (44), which for each partonic channel  $I$  yields

$$\tilde{M}_2(\rho^I) = -\log_2 \left( \frac{(\tilde{A}^I)^4 + (\tilde{C}_z^I)^4 + 2(\tilde{C}_{\perp}^I)^4}{(\tilde{A}^I)^2[\tilde{A}^I]^2 + (\tilde{C}_z^I)^2 + 2(\tilde{C}_{\perp}^I)^2} \right).\tag{75}$$

Results are shown in figure 5. We see that the magic vanishes close to threshold ( $\beta \rightarrow 0$ ) in both channels. Indeed, the analytic forms of the  $R$ -matrices are found to be

$$R^{q\bar{q}}(0) \propto \begin{pmatrix} 1 & 0 & 0 & 0 \\ 0 & 0 & 0 & 0 \\ 0 & 0 & 0 & 0 \\ 0 & 0 & 0 & 1 \end{pmatrix}, \quad R^{gg}(0) \propto \begin{pmatrix} 0 & 0 & 0 & 0 \\ 0 & 1 & -1 & 0 \\ 0 & -1 & 1 & 0 \\ 0 & 0 & 0 & 0 \end{pmatrix},\tag{76}$$

such that the quantum states can be written (using similar methods to section 3.2) as

$$R^{q\bar{q}}(0) \propto \frac{|\uparrow\uparrow\rangle\langle\uparrow\uparrow| + |\downarrow\downarrow\rangle\langle\downarrow\downarrow|}{\sqrt{2}}, \quad R^{gg}(0) \propto |\tilde{\Psi}^-\rangle\langle\tilde{\Psi}^-|, \quad |\tilde{\Psi}^-\rangle = \frac{|\downarrow\uparrow\rangle - |\uparrow\downarrow\rangle}{\sqrt{2}},\tag{77}$$

where we have used  $|\uparrow\rangle$  and  $|\downarrow\rangle$  to denote single qubit spin up and down states along the beam direction. We note that it may seem surprising from figure 3(a) that an angular average of the magic in the  $q\bar{q}$  channel leads to a zero result at  $\beta = 0$ , given that there are clearly non-zero values

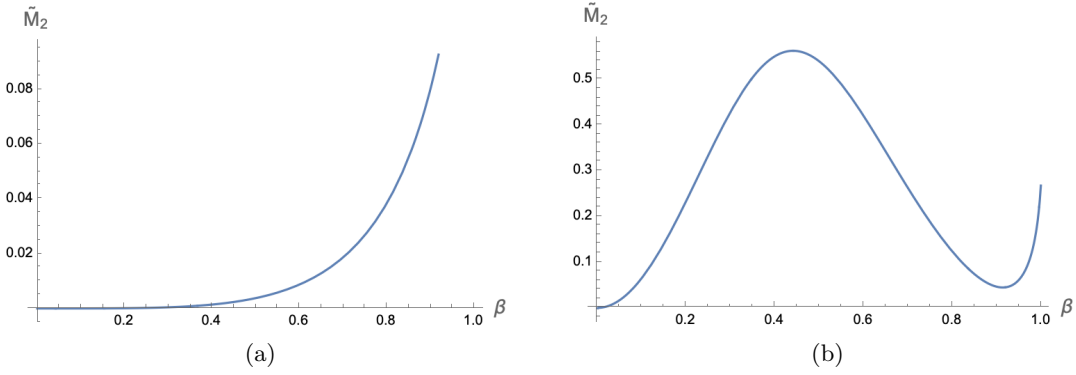


Figure 5: The magic of an angular-averaged mixed top-antitop final state in: (a) the  $q\bar{q}$  channel; (b) the  $gg$  channel.

of the magic along the line  $\beta = 0$ . However, we remind the reader that we are now calculating the magic in a different basis.

As for the fully differential magic, we may convert the partonic magic with angular-averaging into a hadron-level result using the appropriate analogue of eq. (69). First, one defines weighted combinations of normalised coefficients following eq. (68), starting from the coefficients of the angular-averaged density matrix:

$$C_{ij}^{\text{had.}} = \frac{w_{q\bar{q}}(\beta)\tilde{C}_{ij}^{q\bar{q}}}{\tilde{A}^{q\bar{q}}} + \frac{w_{gg}(\beta)\tilde{C}_{ij}^{gg}}{\tilde{A}^{gg}}, \quad (78)$$

where the relevant partonic weights are now functions only of  $\beta$ , due to being defined (similarly to eq. (67)) in terms of angular-averaged quantities:

$$w_I(M) = \frac{L^I(M)\tilde{A}^I(M)}{\sum_J L^J(M)\tilde{A}^J(M)}. \quad (79)$$

The hadronic angular-averaged magic is then given by

$$\tilde{M}_2^{\text{had.}}(\rho) = -\log_2 \left( \frac{1 + [C_z^{\text{had.}}]^4 + 2[C_\perp^{\text{had.}}]^4}{1 + [C_z^{\text{had.}}]^2 + 2[C_\perp^{\text{had.}}]^2} \right). \quad (80)$$

Results are shown in figure 6, and we note the interesting feature that the magic is non-zero for all values of  $\beta$ . This is similar to the behaviour already observed for the fully differential magic, namely that some regions of vanishing magic do not survive upon forming the hadronic result. The underlying mechanism is indeed similar: superposing states from different partonic channels leads to removal of pure stabiliser combinations, and hence increasing magic. The results of this section are still differential in the top quark invariant mass, and one may go further in defining a total top quark final state by integrating over a range of invariant masses e.g. all possible values of  $\beta$ , or some suitable fiducial range. Given that angular averaging already removes all regions of non-zero magic, however, we do not foresee any qualitative difference upon the further mixing of states that occurs upon performing additional integrations.

Another interesting feature of figure 6 is that the region of maximum magic is typically close to threshold (low values of  $\beta$ ), despite the fact that the magic vanishes in this region for each partonic

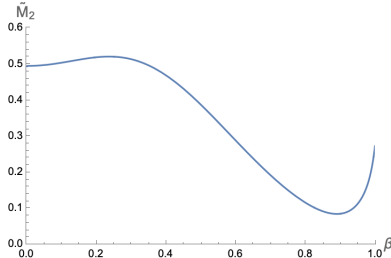


Figure 6: The magic of a mixed angular-averaged top-antitop final state at hadron level.

channel separately. As mentioned previously, the generation of non-zero magic results from combining non-equal stabiliser states with non-integer weights. Our results are also consistent with ref. [5], which shows that top quark entanglement (as measured by the so-called *concurrence*) is no longer maximal in any region once angular averaging has taken place. Given that maximal entanglement is associated with a stabiliser state, this again suggests that the magic will be everywhere non-zero.

## 4 Conclusions

In this paper, we have performed a case study of the *magic*, a property that characterises how different quantum states are from a restricted set of so-called *stabiliser states*. Non-stabiliser states are crucial for designing quantum computers that have a genuine computational advantage over their classical counterparts, and also for fault-tolerant algorithms. Learning how to quantify and control magic in real-world quantum systems are both open problems, such that it makes sense to ascertain whether magic is manifest in the quantum playground offered by collider physics experiments.

We have focused on (anti-)top quark pair production at the LHC, which has recently been the subject of many studies examining top quark entanglement. Magic offers a complementary view to entanglement, in that maximally entangled states typically have zero magic. We find that magic top pairs are generically produced, where the amount of magic depends on the kinematics (i.e. the scattering angle and invariant mass). In each separate partonic channel, regions of zero magic appear, that can be directly traced to the fact that the top quark final state becomes a stabiliser state, which may or may not be entangled. These regions tend to disappear upon combining channels to form the proton-level process, or when averaging over top quark directions. This makes sense, given that combining different states (including individual stabiliser states) will generically result in states which are non-stabiliser, and thus have non-zero magic. Interestingly, the highest magic at angular-averaged level is found close to threshold, where the magic vanishes in each separate channel. As we have discussed in detail, this is a direct consequence of the non-integer partonic weights multiplying each (stabiliser) state.

There are many possible directions for future work. First, one might look at the effect of theories beyond the Standard Model (as has been done for entanglement in ref. [5]), in order to see whether magic is useful as an observable that distinguishes new physics from old. If the SSRE is insufficient, one could consider higher order Stabiliser Rényi entropies as additional observables. We hope in addition that our results will prove useful in informing a more general body of work mapping ideas from quantum computation / information theory to collider physics, where there are presumably

many exciting interdisciplinary insights to be uncovered.

## Acknowledgments

CDW is supported by the UK Science and Technology Facilities Council (STFC) Consolidated Grant ST/P000754/1 “String theory, gauge theory and duality”. MJW is supported by the Australian Research Council grants CE200100008 and DP220100007.

## References

- [1] R. P. Poplavskii, “Thermodynamic models of information processes,” *Phys. Usp.* **18** (1975), no. 3, 222–241.
- [2] M. A. Nielsen and I. L. Chuang, *Quantum Computation and Quantum Information*. Cambridge University Press, 6, 2012.
- [3] Y. Afik and J. R. M. n. de Nova, “Entanglement and quantum tomography with top quarks at the LHC,” *Eur. Phys. J. Plus* **136** (2021), no. 9, 907, 2003.02280.
- [4] Y. Afik and J. R. M. n. de Nova, “Quantum information with top quarks in QCD,” *Quantum* **6** (2022) 820, 2203.05582.
- [5] R. Aoude, E. Madge, F. Maltoni, and L. Mantani, “Quantum SMEFT tomography: Top quark pair production at the LHC,” *Phys. Rev. D* **106** (2022), no. 5, 055007, 2203.05619.
- [6] M. Fabbrichesi, R. Floreanini, and G. Panizzo, “Testing Bell Inequalities at the LHC with Top-Quark Pairs,” *Phys. Rev. Lett.* **127** (2021), no. 16, 161801, 2102.11883.
- [7] C. Severi, C. D. E. Boschi, F. Maltoni, and M. Sioli, “Quantum tops at the LHC: from entanglement to Bell inequalities,” *Eur. Phys. J. C* **82** (2022), no. 4, 285, 2110.10112.
- [8] J. A. Aguilar-Saavedra and J. A. Casas, “Improved tests of entanglement and Bell inequalities with LHC tops,” *Eur. Phys. J. C* **82** (2022), no. 8, 666, 2205.00542.
- [9] M. Fabbrichesi, R. Floreanini, and E. Gabrielli, “Constraining new physics in entangled two-qubit systems: top-quark, tau-lepton and photon pairs,” *Eur. Phys. J. C* **83** (2023), no. 2, 162, 2208.11723.
- [10] Y. Afik and J. R. M. n. de Nova, “Quantum Discord and Steering in Top Quarks at the LHC,” *Phys. Rev. Lett.* **130** (2023), no. 22, 221801, 2209.03969.
- [11] C. Severi and E. Vryonidou, “Quantum entanglement and top spin correlations in SMEFT at higher orders,” *JHEP* **01** (2023) 148, 2210.09330.
- [12] L. Mantani, “Quantum SMEFT tomography: top quark pair,” *PoS ICHEP2022* (11, 2022) 858, 2211.03428.
- [13] J. A. Aguilar-Saavedra, “Postdecay quantum entanglement in top pair production,” *Phys. Rev. D* **108** (2023), no. 7, 076025, 2307.06991.

- [14] T. Han, M. Low, and T. A. Wu, “Quantum Entanglement and Bell Inequality Violation in Semi-Leptonic Top Decays,” 2310.17696.
- [15] E. L. Simpson, *A new spin on top-quark physics: using angular distributions to probe top-quark properties, and make the first observation of entanglement between quarks*. PhD thesis, Glasgow U., 2024.
- [16] J. A. Aguilar-Saavedra, “A closer look at post-decay  $t\bar{t}$  entanglement,” *Phys. Rev. D* **109** (2024), no. 9, 096027, 2401.10988.
- [17] F. Maltoni, C. Severi, S. Tentori, and E. Vryonidou, “Quantum tops at circular lepton colliders,” 2404.08049.
- [18] **ATLAS** Collaboration, “Observation of quantum entanglement in top-quark pair production using  $pp$  collisions of  $\sqrt{s} = 13\sqrt{\text{TeV}}$  with the ATLAS detector,”.
- [19] **ATLAS** Collaboration, G. Aad *et al.*, “Observation of quantum entanglement in top-quark pairs using the ATLAS detector,” 2311.07288.
- [20] **CMS** Collaboration, “Probing entanglement in top quark production with the CMS detector,”.
- [21] A. J. Barr, M. Fabbrichesi, R. Floreanini, E. Gabrielli, and L. Marzola, “Quantum entanglement and Bell inequality violation at colliders,” 2402.07972.
- [22] M. Beverland, E. Campbell, M. Howard, and V. Kliuchnikov, “Lower bounds on the non-clifford resources for quantum computations,” *Quantum Science and Technology* **5** (may, 2020) 035009.
- [23] J. Jiang and X. Wang, “Lower bound for the  $t$  count via unitary stabilizer nullity,” *Phys. Rev. Appl.* **19** (Mar, 2023) 034052.
- [24] L. Leone, S. F. E. Oliviero, and A. Hamma, “Learning t-doped stabilizer states,” 5, 2023. 2305.15398.
- [25] H. Qassim, H. Pashayan, and D. Gosset, “Improved upper bounds on the stabilizer rank of magic states,” *Quantum* **5** (Dec., 2021) 606.
- [26] L. Leone, S. F. E. Oliviero, and A. Hamma, “Stabilizer rényi entropy,” *Phys. Rev. Lett.* **128** (Feb, 2022) 050402.
- [27] T. Haug, S. Lee, and M. S. Kim, “Efficient stabilizer entropies for quantum computers,” 2305.19152.
- [28] S. F. E. Oliviero, L. Leone, A. Hamma, and S. Lloyd, “Measuring magic on a quantum processor,” *npj Quantum Information* **8** (2022), no. 1, 148.
- [29] X. Turkeshi, M. Schirò, and P. Sierant, “Measuring nonstabilizerness via multifractal flatness,” *Phys. Rev. A* **108** (Oct, 2023) 042408.
- [30] A. Gu, L. Leone, S. Ghosh, J. Eisert, S. Yelin, and Y. Quek, “A little magic means a lot,” 2308.16228.

- [31] E. Tirrito, P. S. Tarabunga, G. Lami, T. Chanda, L. Leone, S. F. E. Oliviero, M. Dalmonte, M. Collura, and A. Hamma, “Quantifying non-stabilizerness through entanglement spectrum flatness,” 2304.01175.
- [32] X. Turkeshi, A. Dymarsky, and P. Sierant, “Pauli Spectrum and Magic of Typical Quantum Many-Body States,” 2312.11631.
- [33] P. Shor, “Algorithms for quantum computation: discrete logarithms and factoring,” in *Proceedings 35th Annual Symposium on Foundations of Computer Science*, pp. 124–134. 1994.
- [34] P. W. Shor, “Polynomial-time algorithms for prime factorization and discrete logarithms on a quantum computer,” *SIAM Journal on Computing* **26** (1997), no. 5, 1484–1509, <https://doi.org/10.1137/S0097539795293172>.
- [35] D. Gottesman, “The Heisenberg representation of quantum computers,” in *22nd International Colloquium on Group Theoretical Methods in Physics*, pp. 32–43. 7, 1998. [quant-ph/9807006](https://arxiv.org/abs/quant-ph/9807006).
- [36] P. Niroula, C. D. White, Q. Wang, S. Johri, D. Zhu, C. Monroe, C. Noel, and M. J. Gullans, “Phase transition in magic with random quantum circuits,” 2304.10481.
- [37] S. Aaronson and D. Gottesman, “Improved simulation of stabilizer circuits,” *Phys. Rev. A* **70** (2004), no. 5, 052328, [quant-ph/0406196](https://arxiv.org/abs/quant-ph/0406196).
- [38] L. Leone, S. F. E. Oliviero, and A. Hamma, “Stabilizer Rényi Entropy,” *Phys. Rev. Lett.* **128** (2022), no. 5, 050402, [2106.12587](https://arxiv.org/abs/2106.12587).
- [39] M. Baumgart and B. Tweedie, “A New Twist on Top Quark Spin Correlations,” *JHEP* **03** (2013) 117, [1212.4888](https://arxiv.org/abs/1212.4888).
- [40] D. B. Clark, E. Godat, and F. I. Olness, “ManeParse : A Mathematica reader for Parton Distribution Functions,” *Comput. Phys. Commun.* **216** (2017) 126–137, [1605.08012](https://arxiv.org/abs/1605.08012).
- [41] **NNPDF** Collaboration, R. D. Ball *et al.*, “The path to proton structure at 1% accuracy,” *Eur. Phys. J. C* **82** (2022), no. 5, 428, [2109.02653](https://arxiv.org/abs/2109.02653).
- [42] A. Buckley, J. Ferrando, S. Lloyd, K. Nordström, B. Page, M. Rüfenacht, M. Schönherr, and G. Watt, “LHAPDF6: parton density access in the LHC precision era,” *Eur. Phys. J. C* **75** (2015) 132, [1412.7420](https://arxiv.org/abs/1412.7420).